Carcinogenesis, 2019, Vol. 40, No. 10, 1179–1190

doi:10.1093/carcin/bgz118
Advance Access Publication June 18, 2019
Original Article

ORIGINAL ARTICLE

The *H1047R PIK3CA* oncogene induces a senescence-like state, pleiotropy and acute HSP90 dependency in HER2+ mammary epithelial cells

Anindita Chakrabarty*, Sreeraj Surendran, Neil E.Bhola[1], Vishnu S.Mishra, Tasaduq Hussain Wani, Khemraj S.Baghel, Carlos L.Arteaga[2], Rohini Garg and Goutam Chowdhury[3,4]

Department of Life Sciences, Shiv Nadar University, Uttar Pradesh 201314, India, [1]IDEAYA Biosciences, South San Francisco, CA 94080, USA, [2]University of Texas Southwestern and Simmons Comprehensive Cancer Center, Dallas, TX 75390, USA and [3]Department of Chemistry, Shiv Nadar University, Uttar Pradesh 201314, India [4]Present address: Baghbazar, Kolkata, West Bengal 700003, India

*To whom correspondence should be addressed. Tel: +91 120 381 9100 ext. 282; Email: anindita.chakrabarty@snu.edu.in

Abstract

In pre-clinical models, co-existence of *Human Epidermal Growth Factor Receptor-2* (*HER2*)-amplification and PI3K catalytic subunit (PIK3CA) mutations results in aggressive, anti-HER2 therapy-resistant breast tumors. This is not always reflected in clinical setting. We speculated that the complex interaction between the *HER2* and *PIK3CA* oncogenes is responsible for such inconsistency. We performed series of biochemical, molecular and cellular assays on genetically engineered isogenic mammary epithelial cell lines and breast cancer cells expressing both oncogenes. *In vitro* observations were validated in xenografts models. We showed that H1047R, one of the most common PIK3CA mutations, is responsible for endowing a senescence-like state in mammary epithelial cells overexpressing HER2. Instead of imposing a permanent growth arrest characteristic of oncogene-induced senescence, the proteome secreted by the mutant cells promotes stem cell enrichment, angiogenesis, epithelial-to-mesenchymal transition, altered immune surveillance and acute vulnerability toward HSP90 inhibition. We inferred that the pleiotropism, as observed here, conferred by the mutated oncogene, depending on the host microenvironment, contributes to conflicting pre-clinical and clinical characteristics of HER2+, mutated PIK3CA-bearing tumor cells. We also came up with a plausible model for evolution of breast tumors from mammary epithelial cells harboring these two molecular lesions.

Introduction

The *Human Epidermal Growth Factor Receptor 2 (HER2)* oncogene is amplified and/or overexpressed in ~25% of breast cancers (BC) (1). In tumor cells, HER2 heterodimerizes with kinase-deficient HER3, preferentially activating the phosphatidylinositol 3-kinase (PI3K) intracellular signaling pathway (2).

The PI3Ks are lipid kinases that control cell growth and survival, response to nutrient availability, energy metabolism, migration and invasion (3). Stimulation of class I_A PI3K (heterodimer of 110KDa catalytic subunit and 85KDa regulatory subunit) leads to activation of downstream effector proteins like AKT and mTORC1 (3).

Mutations in the major cancer driver oncogenes such as *EGFR*, *RAS*, *RAF* located in the same signal transduction pathway are often mutually exclusive because their co-existence does not provide any additional benefit to tumor cells (4). Contrary to this expectation, cancer genome analysis revealed common alterations within the PI3K pathway downstream of HER2 in human BC, with up to 39% being the gain-of-function missense

Received: March 1, 2019; **Revised:** May 27, 2019; **Accepted:** June 17, 2019

Abbreviations

BC	breast cancers
CM	conditioned media
EMT	epithelial–mesenchymal transition
HER2	human epidermal growth factor receptor 2
HRG	heregulin
MMP	matrix metalloproteinases
NF-κβ	nuclear factor kappa light chain enhancer of activated B
PBMC	peripheral blood mononuclear cell
PI3K	phosphatidylinositol 3-kinase
ROS	reactive oxygen species
SA-βgal	senescence-associated-βgalactosidase
SASP	senescence-associated secretory proteome
WT	wild-type

mutations within the catalytic subunit of type I_A PI3K (PIK3CA) (5). Majority of these mutations resides at the hotspots within the helical and kinase domains of PIK3CA, particularly at H1047R and E545K/E542K (6). Co-occurrence of mutated *PIK3CA* in *HER2*-amplified BC implies that together these oncogenes provide better selective advantage for the tumor cells than that granted individually. Independent studies clearly demonstrated co-operativity between HER2 and mutated PIK3CA leading to enhanced *in vitro* cell transformation and *in vivo* tumorigenicity along with dampened sensitivity toward anti-HER2 drug like trastuzumab (7,8). In clinic though, effect of the *PIK3CA* mutation on HER2+ BC does not follow these pre-clinical patterns (9). In early-stage HER2+ BC patients receiving neoadjuvant anti-HER2 therapies, *PIK3CA* mutations are associated with significantly lower rate of pathological complete response but not with inferior clinical outcome. Whereas, in metastatic setting, these mutations bear no association with the magnitude of response to anti-HER2 adjuvant therapy but result in worse prognosis.

The underlying reasons for this paradox are unknown, but may be explained by how these two oncogenes interact. The most noteworthy study that attempted to look into this was the bi-transgenic mouse mammary tumor model of *H1047R*-mutated *PIK3CA* and *HER2* oncogenes (8), in which a causal relationship between mutated *PIK3CA* and a stem cell–enriched, epithelial–mesenchymal transition (EMT) phenotype of HER2+ mammary tumors (with a molecular signature resembling Claudin-low BC) was established. However, the inconsistencies between the clinical and pre-clinical properties are not explainable by this model.

Herein, we attempted to clarify how gain of somatic mutations in *PIK3CA* oncogene endows variable characteristics of *HER2*-amplified mammary epithelial cells in different settings. We uncovered a mechanism that not only explains the enrichment of stem and EMT-associated properties in HER2+ and mutated-PIK3CA-expressing cells, also helps to construct a plausible evolutionary roadmap of breast tumorigenesis and an explanation for the differences in the clinical and pre-clinical findings. We also came across a therapeutic strategy different from the standard HER2 or PI3K-targeted agents for effective management of this particular BC subtype.

Materials and methods

Cell lines, inhibitors and primary antibodies

All cell lines obtained from the American Type Culture Collection/ATCC (Manassas, VA) were authenticated by short tandem repeat profiling from Lifecode Technologies (New Delhi, India). The authentication is repeated once in 2 years. Stable clones of MCF10A/WT and HR PIK3CA with or without HER2 were generated and characterized for oncogene expression as described in ref. (7). Inhibitors were procured from Selleckchem and ApexBio, Houston, TX. Fluorescent-tagged CD44, CD24 and CD271 antibodies were purchased from BD Biosciences (Franklin Lakes, NJ). All other primary antibodies, except for HSP90 (Enzo Lifesciences, Farmingdale, NY), were procured through Cell Signaling Technology (Danvers, MA).

Cell proliferation/viability, immunoblot, siRNA and plasmid DNA transfection experiments

Cell proliferation/viability and 3D growth assays were performed as in ref. (7). For population doubling time calculation, cell proliferation was measured at 24, 48 and 72 h post-seeding using the formula: Doubling time = duration × log(2)/log (final concentration) – log (initial concentration). DNA synthesis was measured by BrdU colorimetric immunoassay kit (Sigma–Aldrich, St. Louis, MO). For immunoblot analysis and transfection, protocol from (7) was used. The p110α shRNA and HSP90 siRNA were procured from Santa Cruz Biotechnology (Dallas, TX).

Boyden chamber and mammosphere assays

Boyden chamber migration and invasion assays were performed as in ref. (7). Mammosphere assay was performed as in ref. (8). For self-renewal assays, spheres were enzymatically dissociated into single-cell suspensions and plated at higher dilutions.

Senescence-associated βgalactosidase, comet, GSH measurement assays, immunofluorescence and invadopodia assays

All these experiments were performed as described in refs (10,11).

Quantitative RT-PCR, enzyme-linked immunosorbent assay, proteome Profiler arrays, flow cytometry, zymography, mass spectrometric detection of 8-oxodG, microarray and animal studies

Details are included in Supplementary Material.

Statistical analysis

GraphPad Prism v5.03 (San Diego, CA) was used for statistical analyses (two-tailed, non-parametric t-test). Each bar graph is mean of three to four biological replicates along with standard error. Level of significance for individual experiment (where appropriate) is included in the respective figure legend.

Ethics approval

All animal studies except for the 17-AAG drug treatment study were approved and performed in accordance with the Vanderbilt University Institutional Animal Care and Use Committee guidelines. The 17-AAG study was outsourced to the Advanced Center for Treatment, Research and Education in Cancer (ACTERC), Navi Mumbai, India and conducted according to institutional guidelines.

Results

Co-expression of HER2 and H1047R PIK3CA in MCF10A mammary epithelial and BC cells promotes gain of stem cell–associated properties

We utilized previously characterized isogenic MCF10A cell line series that stably overexpress wild-type (WT) or H1047R

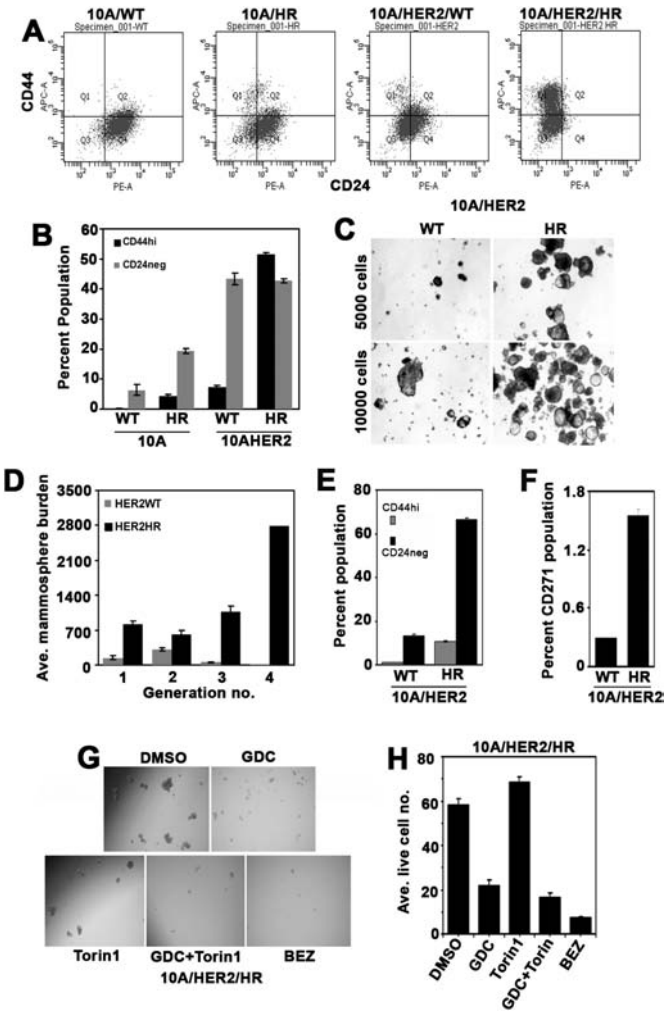

Figure 1. Co-expression of H1047R (HR) PIK3CA in HER2-overexpressing mammary epithelial cell line (MCF10A/HER2) enriches for cells expressing BCSC-associated markers and possessing self-renewal and differentiation abilities. (**A**) and (**B**) FACS analysis for $CD44^{hi}/CD24^{neg}$ population in MCF10A/HER2/HR versus MCF10A/WT, MCF10A/HR and MCF10A/HER2/WT/PIK3CA cell lines. (B) Quantitation of (A). (**C**) and (**D**) Mammosphere assay testing self-renewal and differentiation abilities of MCF10A/HER2/HR compared with MCF10A/HER2/WT cell lines. (C) represents the images (20×) of the spheres formed from MCF10A/HER2/WT and MCF10A/HER2/HR PIK3CA lines when seeded at 5000 versus 10 000 cell/well density. (D) Comparison of the burden of mammospheres (burden = number x volume) formed consecutively over first, second, third and fourth generations from these two cell lines. (**E**) FACS analysis for $CD44^{hi}/CD24^{neg}$ population in serum and growth factor-starved conditions in MCF10A/HER2/HR and MCF10A/HER2/WT cells. (**F**) FACS analysis for of CD271+ cell populations in MCF10A/HER2/HR versus MCF10A/HER2/WT cell lines. (**G**) and (**H**) Effects of PI3K and mTOR inhibitors on mammosphere formation (images at 10×) by MCF10A/HER2/HR cells. (H) Quantitation of cells contributing to sphere formation following treatment with inhibitors for PI3K (GDC-0941; 150 nM), mTOR kinase (Torin-1; 15 nM), PI3K plus mTOR (GDC plus Torin-1 or BEZ-235; 10 nM). Average cell number difference from spheres treated with GDC plus BEZ is statistically significant (at $P < 0.05$) from that with GDC alone ($P = 0.0231$), while the difference between GDC and GDC plus Torin-1 treatment is insignificant ($P = 0.4156$). Bar graphs in (B), (E) and (F) represent average values of at two replicates plus standard deviations.

(HR)-mutated PIK3CA in the absence or presence of HER2 (7). In these models, the co-operativity between the HR-mutated PIK3CA and HER2 oncogenes was established and validated (7). Using FACS analysis, we found a gradual increase in the expression of conventional BCSC marker (12), $CD44^{hi}/CD24^{neg}$ (Figure 1A and B) with the highest expression being associated with both HR PIK3CA and HER2. Comparison of the sphere forming abilities (as a readout of the stem cell–associated self-renewal and differentiation properties (13)) confirmed the HER2/HR-expressing cell line to be more enriched for stem-like cells (Figure 1C and D).

Maintenance of the non-cancerous mammary epithelial origin MCF10A cell line requires addition of serum and exogenous growth factors (14). Previously, we demonstrated that introduction of *HR PIK3CA* oncogene in MCF10A/HER2 cells relieves dependency on such exogenous factors, partly through the secretion of HER3 ligand heregulin (HRG) (7). Interestingly, HRG is also linked to enhanced sphere formation through activation of PI3K/NF-κβ signaling axis (15). Therefore, to correlate growth factor independency of MCF10A/HER2/HR PIK3CA-expressing cells with stem cell–enriched phenotype, we checked for CSC marker expression under conditions of serum and growth factor starvation. For normalization we started with equal number of cells for both lines. Up to 10-fold increase in populations with $CD44^{hi}$ and 6-fold increase in populations with $CD24^{neg}$ expressions were observed in starved mutant cells than those in WT cells (Figure 1E). We also used CD271, an alternative surface antigen specific for mammary epithelial cells possessing tumor-initiating/stem-like properties (16) and found at least 5-fold increase in CD271+ population in MCF10A/HER2/HR cells (Figure 1F).

We went on to confirm the 'stem cell–enriched' phenotype in HER2+ and *HR PIK3CA* oncogene-expressing BC cells. In cell

lines of both basal (BT-20) and luminal (T47-D) mammary epithelium origin, co-expression of mutated PIK3CA and HER2 (Supplementary Figure S1A, B and D, available at *Carcinogenesis* online) resulted in clear-cut increase in $CD44^{hi}/CD24^{lo}$ population with high aldehyde dehydrogenase activity ($ALDH1^{+}$), another marker for BCSCs (17) (Supplementary Figure S1C and E, available at *Carcinogenesis* online). Although, $CD44^{hi}/CD24^{lo}$ are less rigorous markers than that of $CD44^{hi}/CD24^{neg}$ (Figure 1), a combination of three markers $ALDH^{+}/CD44^{hi}/CD24^{lo}$ offered the most stringent *in vitro* condition for BCSC identification. In fact, cells expressing all three markers together are thought to be the rarest, possessing the greatest tumor-initiating capacity in cancer models (18). Unlike the MCF10A mammary epithelial cell line, both BT-20 and T47-D cell lines are p53-mutated (https://portals.broadinstitute.org/ccle), yet demonstrated similar trend toward enrichment of stem cell–associated markers when engineered to co-express HER2 and HR PIK3CA, indicating that this phenomenon is independent of p53 status.

Neither MCF10A/HER2/WT nor MCF10A/HER2/HR cells form tumors in NOD/SCID mice. Because tumor emergence at a very low density in severely immunocompromised mice is a gold-standard test for confirming tumor-initiating capacities of cancer stem cells (19), we carried out xenotransplantation experiments with T47-D cells plus/minus engineered HER2. While, inoculation of 10 000 cells resulted in no difference in tumor incidence between T47-D/HER2 and T47-D/pCDNA groups, with 100 cells, the tumor-forming efficiency of T47-D/HER2 cells was higher than that of T47-D/pCDNA cells (83 versus 60%) (Supplementary Figure S1F and G, available at *Carcinogenesis* online).

Final confirmation for direct link between HR-mutated PIK3CA and enrichment of BCSC-like population in HER2+ BC cells came from loss-of-function experiments by genetically depleting or pharmacologically inhibiting PI3K in *HER2*-amplified and *HR PIK3CA*-expressing HCC1954 cell line (Supplementary Figure S2, available at *Carcinogenesis* online). Both *in vitro* and *in vivo* RNAi of PIK3CA clearly inhibited the $ALDH^{+}$ population (Supplementary Figure S2A and C, available at *Carcinogenesis* online). Also, pharmacological inhibition of PIK3CA, but not PIK3CB with specific inhibitors INK1117 and TGX221, respectively, resulted in a more effective reduction in PI3K signaling and concomitant decrease in $ALDH^{+}$ population (Supplementary Figure S2D, available at *Carcinogenesis* online). Similarly, treatment of HCC1954 xenografts with XL147, a pan-PI3K inhibitor effectively decreased $ALDH^{+}$ BCSC marker expression (Supplementary Figure S2G, available at *Carcinogenesis* online).

In pre-clinical models of HER2+BC, HR PIK3CA causes hyperactivation of PI3K signaling (7,8). To determine the molecule among PI3K, AKT and mTOR, responsible for BCSC enrichment, we treated the MCF10A/HER2/HR mammospheres with GDC-0941 (PI3K inhibitor), Torin-1 (mTOR kinase inhibitor), a combination of GDC plus Torin-1, and BEZ-235 (PI3K/mTOR dual inhibitor). Inhibition of PI3K, but not mTOR, significantly decreased sphere-forming ability of cells expressing HR PIK3CA (Figure 1G and H). Interestingly, while the combination of GDC plus Torin-1 had little additive effect, BEZ-235, a dual PI3K/TOR inhibitor, prevented sphere formation significantly, which could be attributed to additional effect of this molecule on DNA-damage response signaling (20), which we later found to be operating in these cells. Similar dependency on PI3K, but not mTOR was observed in cell proliferation assays, both in 2D and in 3D, respectively (Supplementary Figure S3A and C, available at *Carcinogenesis* online). All three inhibitors are well characterized for intended target inhibition (21–23).

Expression of HR PIK3CA endorses EMT-like features in HER2+ mammary epithelial and BC cells

Gain of stem-like properties is often associated with EMT, a cellular program that enables cancer cells to migrate, invade and metastasize (24). Also, in mouse models, HR-mutated PIK3CA is known to enhance metastasis of HER2+ mammary tumors (8). Hence, we tested for EMT in the HER2/HR PIK3CA cells along with the WT PIK3CA-bearing cells as control. Microscopic examination revealed a spindle-shaped, highly dispersed, poorly differentiated morphology (indication of EMT (25)) of HR cells compared with the well-differentiated epithelioid appearance of WT cells (Figure 2A). Immunofluorescence and q-PCR experiments to detect loss of epithelial and gain of mesenchymal markers showed reduced expression of molecules associated with cell–cell adhesion (E-cadherin), maintenance of epithelial tight junction (Zona occludens 1) and increased expression of mesenchymal markers (N-cadherin and Vimentin) in HR cells (Figure 2B and C). Additionally, components of extracellular matrix, such as fibronectin, were also increased (Figure 2B and C). In normal epithelial cells, β-catenin, a key component of WNT signaling exists in a membrane-bound fraction as a stable complex with E-cadherin. Upon induction of EMT, this complex undergoes rapid internalization, allowing cellular rearrangements to occur (26). In compliance, we observed a reduction in β-catenin membrane staining and mRNA expression in MCF10A/HER2/HR cells (Figure 2B and C). The expression levels of several EMT-associated transcription factors (SNAIL, TWIST, ZEB1, LEF1, ETS1 and FOXC2) between MCF10A/HER2/HR and WT cells were detected to be at least 2-fold higher in HR cells, with ZEB1 and LEF1 being the most prominent (Figure 2D). Because loss of E-cadherin expression is regulated by the microRNA-200 family members (27), we compared expression levels of miR-200a, b and c between MCF10A/HER2/HR and WT cells and found two out of three to be downregulated in mutant cells (Figure 2E).

EMT helps cancer cells invade through stromal layer and metastasize using specialized enzymes called matrix metalloproteinases (MMP) and form actin-based membrane protrusions called invadopodia (28,29). Because TWIST, the major EMT-specific transcription factors involved in invadopodia formation (30) is upregulated in HR PIK3CA cells (Figure 2D), we compared the ability of WT and HR cells to form invadopodia along with measurement of MMP-2 and -9 activities. These two MMPs can degrade type IV collagen, a major component of the basement membrane secreted by the tumor cells during EMT (31). Along with more prominent invadopodia formation (Figure 2F and Supplementary Figure S4, available at *Carcinogenesis* online), gelatin zymography with equal amount of proteins revealed higher activities of both MMPs in HR cells, compared with WT control (Figure 2G).

Finally, because EMT and CSC are associated with chemotherapy resistance (32), we compared the sensitivities of WT and HR cells toward paclitaxel, an agent beneficial for HER2+ BC (33). As an indirect indication for ongoing EMT, MCF10A/HER2/HR cells deemed less sensitive to paclitaxel than the isogenic WT control (Figure 2H).

Co-expression of HER2 and HR PIK3CA in mammary epithelial cells promotes angiogenic phenotype

CSCs promote tumor vascularization, a process critical for cancer progression (34). Therefore, we assessed the ability of HR cells to support angiogenesis. Using conditioned media (CM) from WT or HR PIK3CA cells (plated at equal density) cultured for 48 h, we performed an antibody array that allows

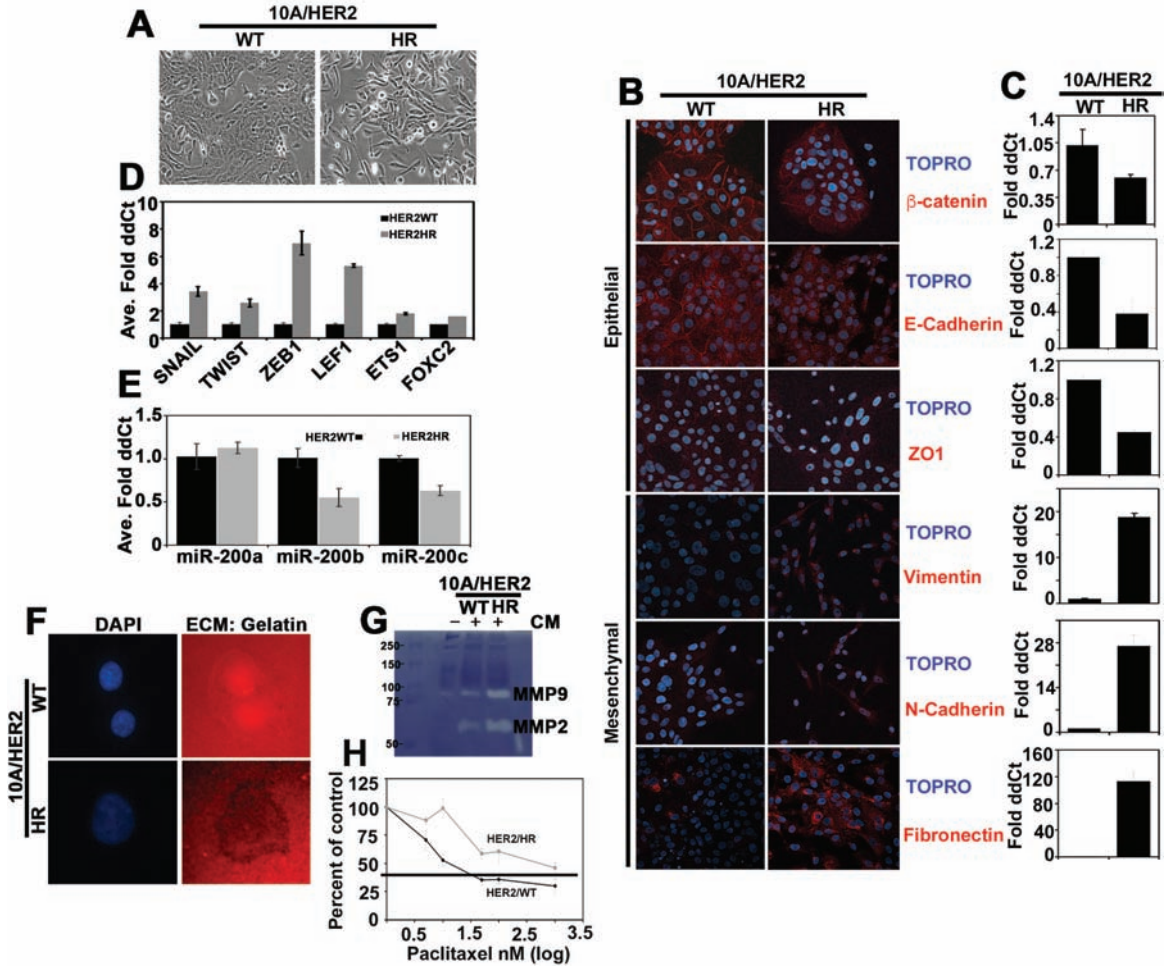

Figure 2. Co-expression of HR PIK3CA and HER2 endorses EMT-like features. (**A**) Light microscopic images (10×) of MCF10A/HER2/WT and HR PIK3CA cell lines grown under standard conditions. Immunofluorescence (**B**; 10×) and q-PCR (**C**) assays for epithelial and mesenchymal marker expression between WT and HR PIK3CA cells. (**D**) Q-PCR assays for EMT-associated transcription factor expression between MCF10A/HER2/WT and HR cell lines. (**E**) Q-PCR assays for EMT-associated miR-200a, b and c in MCF10A/HER2/WT and HR cells. (**F**) Invadopodia formation by MCF10A/HER2/WT and HR cells in gelatin matrix. The black boundary is indicative of matrix degradation (60×). (**G**) Gelatin zymography testing MMP-2 and -9 activities in MCF10A/HER2/WT and HR PIK3CA cells (equal amount of protein loaded for each cell line extract). (**H**) Growth assay displaying differential sensitivities of MCF10A/HER2/WT and HR PIK3CA cells toward increasing doses of paclitaxel over 72 h period. Bar graphs or each point in (C), (D), (E) and (H) represent average values of at least three replicates plus standard errors.

simultaneous detection of 55 human angiogenesis-related molecules. We detected multiple proteins including Angiogenin (ANG), Angiopoietin-1 (Ang-1), EGF, Endoglin, TGF-β1 to be preferentially upregulated in HR cells (Figure 3A). Several of these (TGF-β1 and -β3, IL-8, Endoglin, PAI, PTX-3) were also increased by at least 1.5-fold at the transcript levels (Figure 3B). Noteworthy from these cytokines are TGF-β1 and its auxiliary receptor Endoglin, because TGF-β signaling is implicated both in tumor angiogenesis and EMT, metastasis and maintenance of mammary gland and BC stem cells (35). Consistent with the protein array result, ELISA assay also revealed enhanced secretion of TGF-β1 from HR cells (Figure 3C). Because TGF-β1 is proteolytically activated (36), to determine whether the secreted TGF-β1 is functionally active, we performed dual luciferase reporter assay in cells co-transfected with pCAGA-FLuc and pRL-SV40 constructs. A higher baseline TGF-β1 transcriptional activity dampened by an established TGF-β type I receptor inhibitor, LY2157299 (37) (LY-99), was detected in HR cells than in WT control cells (Figure 3D). The causal relationship between the *HR PIK3CA* oncogenic activity and enhanced TGF-β signaling was further validated by comparing sensitivity towards LY99 alone or in combination with PI3K/mTOR dual-specificity inhibitor, BEZ-235. BEZ alone or in combination with LY-99, but not LY-99 alone, noticeably affected both 3D growth (Figure 3E and Supplementary Figure S5A, available at *Carcinogenesis* online) and sphere-forming ability (Figure 3F and Supplementary Figure S5B, available at *Carcinogenesis* online) of HR cells. Finally, to determine whether angiogenic factors produced by mutant cells support angiogenesis, we performed tube formation assay on human umbilical vein endothelial cells and found subtle, yet enhanced ability of HR-secreted factors to support tube formation within a 12 h period compared with WT control (Supplementary Figure S6, available at *Carcinogenesis* online).

A senescence-like state associated with oxidative DNA damage is prevalent in HER2/HR PIK3CA cells

A two-way cross-talk between tumor cells and their microenvironment through secretion of autocrine and paracrine factors is essential for BCSC maintenance (38). These factors include, but not limited to, interleukins IL-6, IL-8, chemokine MCP-1 and cytokine TGF-β (38). We already have identified a few of these factors upregulated in HR cells (Figure 3A). To further check

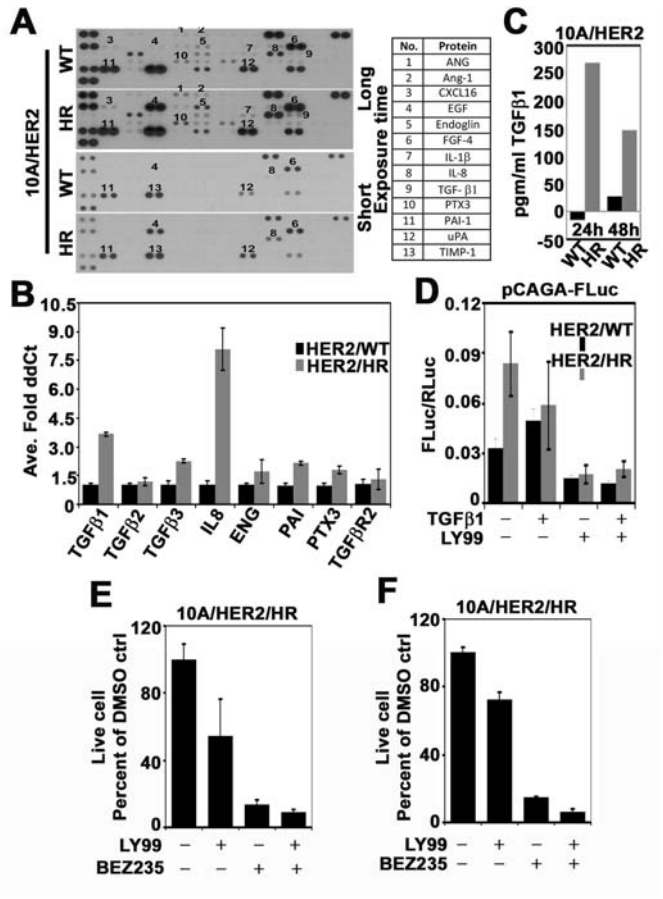

Figure 3. Co-expression of HR PIK3CA and HER2 stimulates angiogenesis-associated marker expression. (**A**) Angiogenesis array hybridized with CM collected from MCF10A/HER2/WT and HR PIK3CA cell lines. Differentially regulated proteins are listed in the tabular format. (**B**) Q-PCR assay for numerous candidates identified in (A). Endogenous TGF-β1 production (**C**) and TGF-β1 pathway activity (**D**) by ELISA (one representative experimental data) and Luciferase (Luc) reporter assays, respectively, from the MCF10A/HER2/WT and HR PIK3CA cell lines. F = firefly and R = renilla luciferase. Results are shown as ratio of F/R Luc activities. Effects of PI3K/TOR (BEZ-235) or TGF-βRI (LY-2157299/LY-99) inhibitor alone or together on 3D (**E**) and mammosphere growth (**F**) of MCF10A/HER2/HR PIK3CA cells. In (E) and (F), concentrations of LY-99 and BEZ-235 are 5 μM and 10 nM, respectively. Bar graphs in (B), (D), (E) and (F) represent average values of at least three replicates plus standard errors.

whether any additional factors can be detectable at higher levels in these cells, we hybridized 48 h CM collected from WT and HR cells (normalized for equal plating density) with a human cytokine array. Several cytokines including IL-6 and IL-8 are upregulated in HR compared with WT CM (Figure 4A). A slight increase in the IL-6 and IL-8 transcript levels was also detected in HR cells (Figure 4B).

At this point, it seemed that the ability to produce a plethora of secretory proteins is one of the major drivers for the gain of phenotypic and functional properties of stem-like population by MCF10A/HER2/HR cells. We wanted to check if these overlap with that produced from cells undergoing growth arrest (senescence) due to activation of potent oncogenes like *RAS* and *RAF* (39). It is noteworthy here, that in addition to enforcing and maintaining senescence, the senescence-associated secretory proteome (SASP) functions in restoring tumorigenesis, promoting metastasis, immune modulation and emergence of CSCs (40). The most predominant of all SASP components are IL-6 and IL-8, which are also upregulated in HR cells (Figures 3A and 4A). Because of one of the major regulators of IL-6 and IL-8 transcription (https://bioinfo.lifl.fr/NF-KB/), transcription factor NF-κβ (nuclear factor kappa light chain enhancer of activated B cells) also regulates senescence (39), we looked for evidence of NF-κβ pathway activation and indeed found upregulation of pp65 NF-κβ (Figure 4C and Supplementary Figure S7A, available at *Carcinogenesis* online) and enhanced reporter expression from a NF-κβ responsive promoter (Figure 4D) in HR cells. To obtain further evidence of senescence in HR cells, we used immunohistochemistry-based measurement of senescence-associated-βgalactosidase (SA-βgal) activity. The MCF10A/HER2/HR cells contained at least a 2-fold greater senescent population than the WT control (Figure 4E and Supplementary Figure S7B, available at *Carcinogenesis* online). Morphologically, senescent cells are flat with a reduced ratio of nuclear staining intensity (with DNA-associated fluorescence dye 4,6-diamidino-2-phenylindole) versus nuclear size (41). Using this parameter, we observed a 3-fold reduction in the ratio of nuclear staining intensity to nuclear area in HR cells compared with WT cells (Supplementary Figure S7C, available at *Carcinogenesis* online). Last, because senescence is associated with growth arrest (39), we compared differences in growth rate between MCF10A/HER2/WT and HR cells and collectively found evidences of moderate growth arrest in HR cells from longer population doubling time (Figure 4F), lesser BrdU incorporation (Figure 4G), moderate G2/M phase arrest (Figure 4H) and upregulation of cell cycle inhibitors CIP-1/p21 and KIP-1/p27 (Figure 4I).

Senescence depends on chronic DNA damage response through generation of reactive oxygen species (ROS) (42). Indeed,

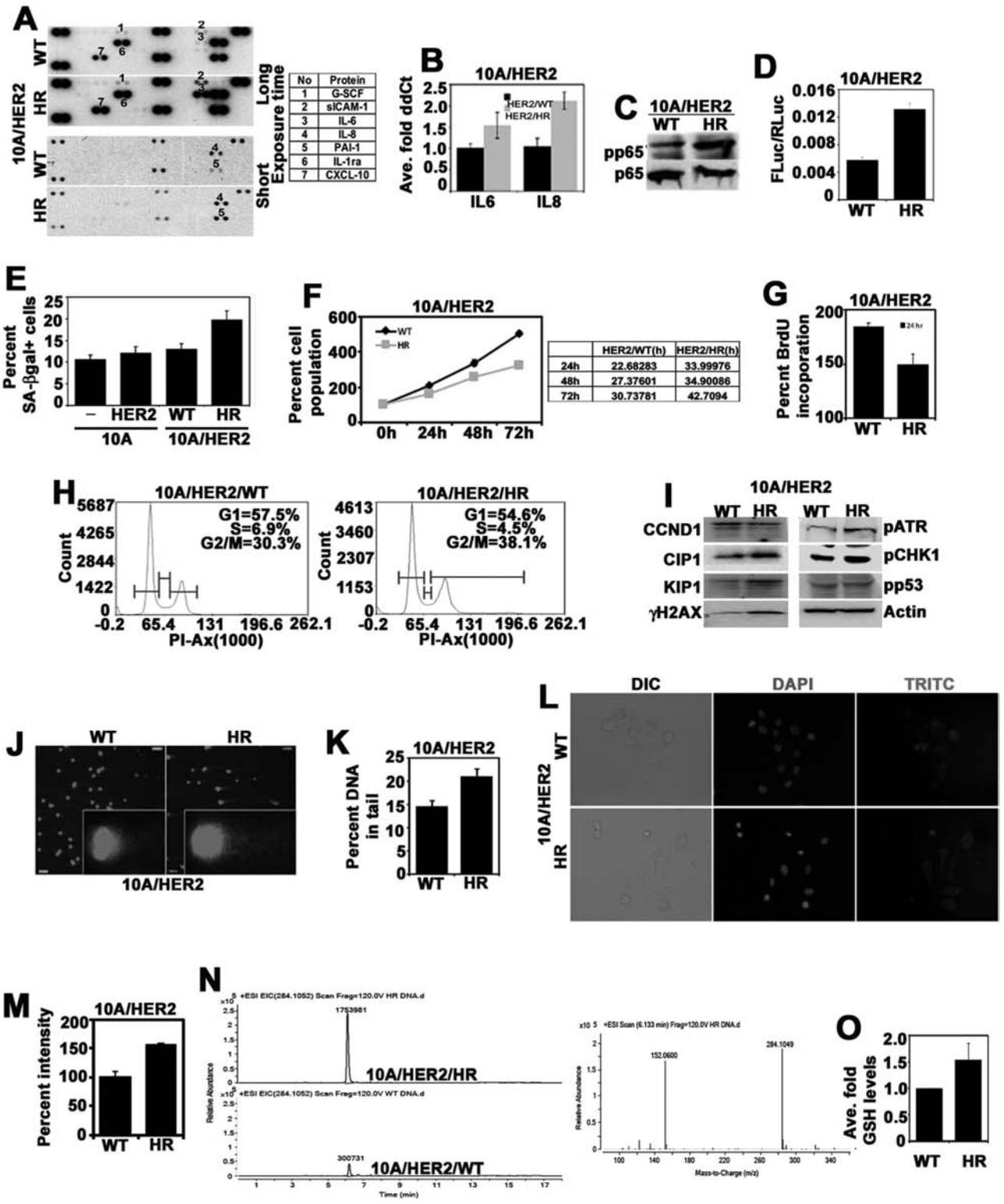

Figure 4. Co-expression of HR PIK3CA and HER2 promotes senescence-like phenotype in MCF10A/HER2 cells due to persistent DNA-damage response. (**A**) Cytokine array hybridized with CM collected from MCF10A/HER2/WT and HR PIK3CA-expressing cell lines. Each differentially regulated cytokine is marked. (**B**) Q-PCR assay for candidates identified in (A). Immunoblot analysis (**C**) and Luc reporter assays (**D**) for NF-κβ pathway activation in MCF10A/HER2/WT and HR PIK3CA-expressing cells. (**E**) Immunohistochemical assays detecting senescence marker SA-βgal activity in MCF10A cells bearing both *HER2* and *HR PIK3CA* oncogenes. Differences in percent SA-βgal+ population between MCF10A/HER2/WT and HR PIK3CA cells is statistically significant ($P = 0.00997$). (**F**) and (**H**) Comparison of growth rate between MCF10A/HER2/WT and HR PIK3CA cells by measuring population doubling time (F), BrdU incorporation (**G**) and cell cycle analysis by FACS (H). (**I**) Immunoblot analysis for cyclin D1 (CCDNA1), CIP1, KIP1, γH2AX, pATR, pCHK1, pp53 and Actin (loading control) in MCF10A/HER2/WT and HR PIK3CA cell extracts. (**J**) and (**K**) Comet assay for detection of DNA damage in MCF10A/HER2/WT and HR cells. (K) is the quantitation of the tail length (indicative of extent of DNA damage) from (**J**) (10× magnification). (**L**) and (**M**) Immunofluorescence assay measuring ROS production in WT versus HR mutant MCF10A/HER2 cells. (M) is the quantitation of (L) (40× magnification) following ImageJ analysis. (**N**) MS detection of oxidative DNA damage marker 8-oxodG spontaneously formed in MCF10A/HER2/WT versus HR cells. Right-hand panel shows the MS-MS data. (**O**) Measurement of total GSH levels in WT and HR cells. Bar graphs in (B), (D), (E), (G), (K) and (M) represent average values of at least three replicates plus standard errors. Bar graph in (O) represents average value of two independent measurements plus standard deviation.

evidences of subtle, yet persistently higher baseline DNA damage, ROS production, oxidative stress and modest increase in DNA-damage response proteins (γH2AX, pATR, pCHK1) were evident in MCF10A/HER2/HR cells by comet and immunofluorescence assays, immunoblot analyses and mass spectrometric detection of oxidative stress-marker 8-oxodeoxyguanosine (43) (Figure 4I–N).

We anticipated the involvement of an altered cellular anti-oxidant defense system for maintaining the oxidative stress and associated DNA damage below a level low enough to not allow full growth arrest settling in the MCF10A/HER2/HR cells. We coined this state as 'senescence-like'. In agreement with our expectation, higher endogenous anti-oxidant GSH levels were evident in HR cells than in WT cells (Figure 4O).

Finally, because we speculated that a senescence-like state and associated secretome are responsible for conferring diverse range of phenotypic and functional properties of *HR PIK3CA* oncogene-expressing cells, the percent senescent populations were also expected to be maintained over multiple generations. Likewise, a stable percentage of βgal+ population was detected in MCF10A/HER2/HR cell line over five consecutive passages (Supplementary Figure S7D, available at *Carcinogenesis* online).

Secretory proteins from MCF10A/HER2/HR PIK3CA cells influence multiple processes of tumorigenesis and immune response

SASP can exert bystander effect on the neighboring non-senescent cells spreading DNA damage, reinforcing senescence or promoting tumorigenesis, metastasis and evading immune surveillance (40,44). We predicted that the HR secretome, having similarity with that of SASP, not only is responsible for pleiotropic effects of the oncogene on HER2-transformed cells, but also is involved in modulating the host microenvironment such as immune cells. Hence, we performed experiments with 48h CM (collected from both WT and HR-expressing cells, plated at equal density) on cells of isogenic and heterogenic origins. As shown in Figure 5A, addition of CM from MCF10A/HER2/HR, but not WT cells increased percentage of SA-βgal+ cells in normal mammary epithelial MCF10A cell line, supported sphere formation and induced morphological changes characteristics of

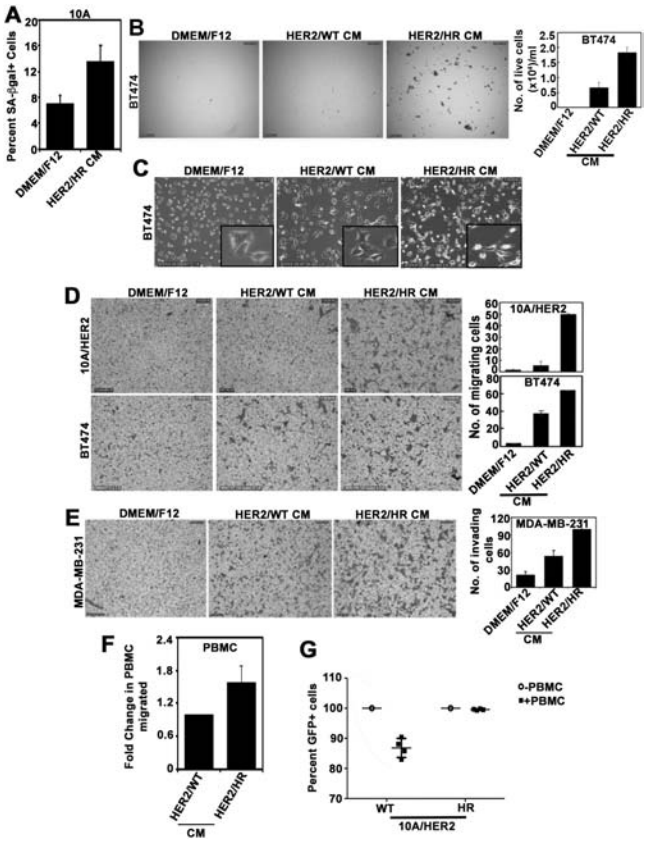

Figure 5. Secretory proteins from MCF10A/HER2/HR PIK3CA cells are enriched with factors enforcing senescence, forming mammospheres, altering cellular morphology, promoting cell migration and invasion, chemoattracting immune cells and modulating immune surveillance. (**A**) Assay for SA-βgal activity in MCF10A cells treated with CM collected from serum and growth factor-starved MCF10A/HER2/HR cells. Dulbecco's modified Eagle's medium (DMEM)/F12 without added serum and growth factor supplements serves as a negative control. (**B**) Mammosphere assay (5×) with BT-474 cells treated with CM collected from MCF10A/HER2/WT and HR PIK3CA cells. Right panel is the quantitation of cells contributed to sphere formation following 14 days of CM treatment. (**C**) Microscopic images (10×) of BT-474 cells treated with DMEM/F12 and CM from MCF10A/HER2/WT and HR PIK3CA cells for 24 h. (**D**) Measurement of transwell migration (10×) of MCF10A/HER2 and BT-474 cells lines following treatment with DMEM/F12 and CM collected from MCF10A/HER2/WT and HR PIK3CA cells. Right panel represents the number of cells migrated under different conditions. (**E**) Measurement of invasiveness (10×) through matrigel-coated transwell chambers of MDA231 cells treated with DMEM/F12 and CM from MCF10A/HER2/WT versus HR PIK3CA cells. Right panel is the quantitation. (**F**) Quantitation of number of monocytes migrated toward CM from MCF10A/HER2/WT versus HR cells in a transwell migration assay. Average values were taken from duplicates and represented with standard deviation. (**G**) Measurement of percent GFP+ cells (MCF10A/HER2/WT or HR) survived following 8 h incubation with PBMC. In (F) and (G), two different sets of PBMC samples were used. Bar graphs represent average values of triplicates plus standard errors unless otherwise mentioned.

invasive cancer cells in BT474, a poorly invasive *HER2*-amplified cell line without highly oncogenic *PIK3CA* mutation like H1047R (Figure 5B and C). Furthermore, in Boyden chamber assays, the same HR CM increased migration of BT474 and MCF10A/HER2 cells (Figure 5D; upper and lower panels) and invasion of *HER2* non-amplified, *PIK3CA* non-mutated MDA231 cells (Figure 5E).

A major function of SASP is to attract immune cells prompting rapid clearance of senescent cells, a process that plays crucial role in tumor suppression (39). However, some of SASP components are also known to influence recruitment and differentiation of circulating monocytes and alter macrophage balance to hinder such immune clearance (40). In the absence of a suitable *in vivo* model at our disposal, we first looked into the ability of the HR CM to attract circulating monocytes from peripheral blood (PBMC). In a Boyden chamber migration assay, two different sets of PBMCs were found to migrate better toward the CM collected from HR cells than that from WT cells (Figure 5F). Next, we performed a co-culture assay of HR and WT cells with five times excess PBMC for 8 h, followed by culturing them up to 24 h and determining their viability by FACS analysis (both MCF10A/HER2/WT and HR cells are GFP+). As shown in Figure 5G and Supplementary Figure S8A and B, available at *Carcinogenesis* online, viability of the HR was less affected by PBMC compared with WT cells, implying that the HR-specific secretome resists clearance of transformed cells by circulating monocytes.

HER2/HR PIK3CA cells are acutely sensitive to HSP90 chaperone inhibition

In pre-clinical models and some clinical specimens of this subtype of BC, limited efficacies of anti-HER2 agents and PI3K pathway inhibitors were reported (45). In fact, in light of our finding that HR PIK3CA-induced senescence-like state confers gain of functional properties of stem cells in HER2+ cells, it is easy to envision why this particular subtype of BC would be insensitive to anti-HER2 therapies. In order to find an alternative therapeutic strategy for HER2+, PIK3CA-mutated cancers, we performed connectivity map (cmap) analysis, a tool able to connect disease conditions with a drug of well-characterized mode of actions (46). For this, first we performed transcriptomic analysis to identify genes that are preferentially altered in mutated cells. A total of 294 differentially expressed probes were identified (126 up and 168 downregulated) (Supplementary Table S1, available at *Carcinogenesis* online: GSE117389), of which *Neuregulin1* (*NRG1*, already known to be abundant in MCF10A/HER2/HR cells (7)) (Supplementary Figure S9, available at *Carcinogenesis* online) was the most upregulated. Upon gene set enrichment analysis of differentially regulated genes with the Molecular Signature Database (MSigDB), we found enrichment of genes possessing H3K27Me3 histone modification signature in embryonic stem cells, genes involved in EMT, metastasis, oncogene-induced senescence, activation of NF-κβ, WNT, TGF-β1 signaling and *KRAS* oncogene (Supplementary Table S2, available at *Carcinogenesis* online). Similarly, biological processes like epidermis development, immune response, inflammation, extracellular structure organization, cell–cell communication, calcium signaling, angiogenesis, wound healing, cytokine biosynthesis and transmembrane transport were among prominent differences between HR and WT cells (Supplementary Table S3, available at *Carcinogenesis* online). Next, by using cmap analysis, we found a strong negative correlation of the HR-specific gene expression signature with that from the cultured cells treated with HSP90 inhibitors Geldanamycin and Tanespimycin (Supplementary Table S4, available at *Carcinogenesis* online). Negative correlation between gene signatures implied that genes typically upregulated in cells expressing HR PIK3CA are downregulated in cultured cancer cell lines upon treatment with HSP90 inhibitors and vice versa. We analyzed previously published gene expression data (GSE41118) of *HER2* and *HR PIK3CA* mouse mammary tumors (8) and discovered very similar correlation (Supplementary Table S4, available at *Carcinogenesis* online). Taken together, we hypothesized that HR PIK3CA prompts a gene expression signature in HER2+ cells that can be reversed by HSP90 inhibition.

This hypothesis was tested by comparing the effect of Tanespimycin/17-AAG on the 2D growth of MCF10A/HER2/WT versus HR cells. As shown in Figure 6A, although 25nM 17-AAG inhibited both WT and HR cells similarly, serum and growth factor-deprivation caused a greater growth inhibition of HR cells (left panel versus right panel). This prompted the speculation that HR-specific secretory factors typically masked by the presence of exogenous serum and growth factors render them more dependent on HSP90 chaperone function. In fact, when compared total protein concentration in equal number of HER2/WT and HR cells, the later seemed to have higher protein (especially structural and secretory) levels (Supplementary Figure S10A and B, available at *Carcinogenesis* online). Next, we determined the effect of 17-AAG on the 3D and sphere growth of MCF10A/HER2/HR (Figure 6B) and HCC1954 cells (Supplementary Figure S10C, available at *Carcinogenesis* online), *in vitro* assays that mimic *in vivo* tumor growth and measure CSC activity, respectively. Both of these properties were drastically inhibited by the 17-AAG treatment.

Because 17-AAG does not alter the expression of HSP90, co-chaperone HSP70 level augmented by 17-AAG is used as its predictive biomarker in cultured cells and patients' samples (47). We confirmed that 17-AAG treatment elevated HSP70 in our models (Figure 6C and Supplementary Figure S10D, available at *Carcinogenesis* online). In order to rule out the possibility that 17-AAG-mediated growth inhibition is not an off-target effect of the drug, we repeated the 3D and sphere-forming assay following RNAi of HSP90 in MCF10A/HER2/HR cells and obtained consistent results (Figure 6D).

As we believed that the HR secretome is the major target of HSP90, its inhibition or genetic ablation should eliminate the senescent population in HER2/HR cell line. It was indeed verified by a drastic reduction in the SA-βgal+ population in siHSP90-transfected MCF10A/HER2/HR cells (Supplementary Figure S10E, available at *Carcinogenesis* online). A direct link between HSP90 and HR secretome was further established due to a drastic reduction in levels of HRG, IL-6, IL-10, MIF and RANTES (through immunoblot and protein array analyses) in siHSP90-transfected cells (Figure 6E and Supplementary Figure S10F, available at *Carcinogenesis* online). In immunoblot, as positive controls, we used HSP90 client proteins HER2 and HER3 (https://www.picard.ch/downloads/Hsp90interactors.pdf), levels of which, both total and phosphorylated, were downregulated in siHSP90-transfected cells (Figure 6E). Because HR cell growth depends largely on HER3 and its endogenous ligand HRG (7), it is possible that the acute growth inhibitory effect of 17-AAG or siHSP90 is partly associated with the inhibition of HER2–HER3 signaling.

In vivo anti-tumor efficacy of 17-AAG was tested by treating HCC1954 xenograft-bearing mice with 17-AAG for one-month which showed a noticeable tumor-static effect (Figure 6F and Supplementary Figure S10G, available at *Carcinogenesis* online) without a significant loss of body weight (Supplementary Figure S10H, available at *Carcinogenesis* online). Also, downregulation of three major HR-specific secretory proteins HRG, IL-6 and IL-8 (Figure 6G–H) and upregulation of HSP70 were demonstrated in 17-AAG-treated tumors (Figure 6G).

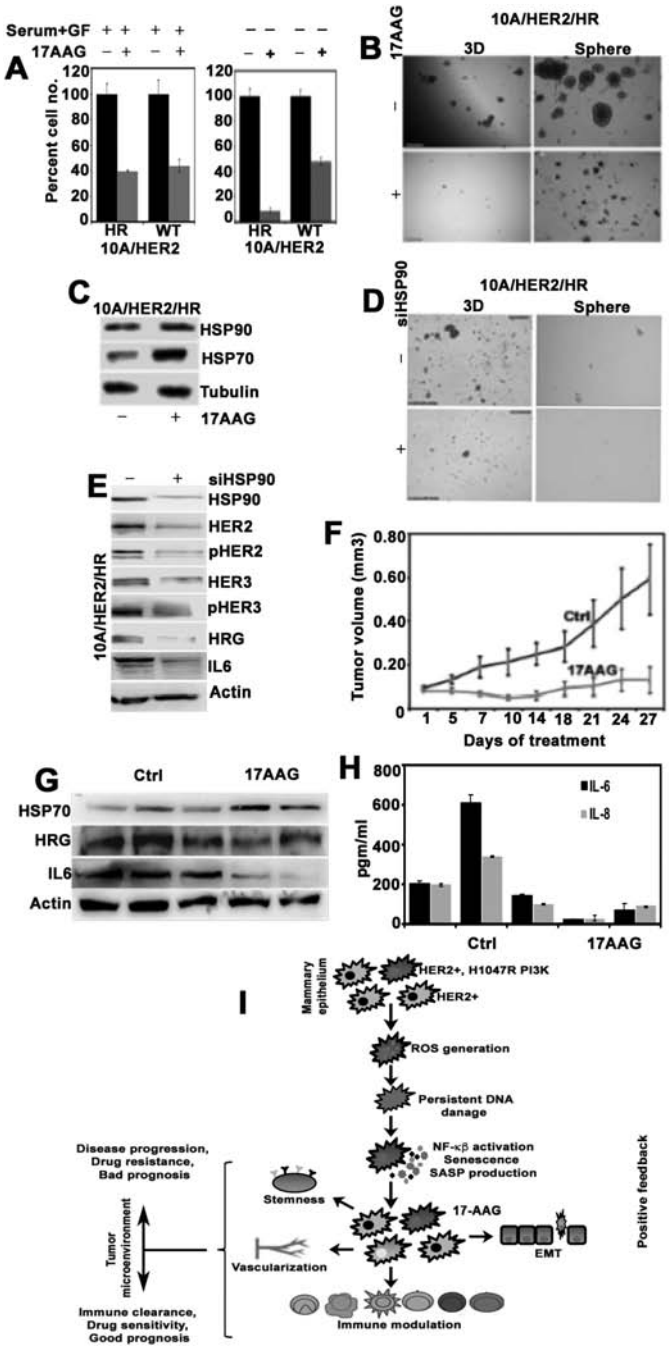

Figure 6. Inhibition of HSP90 acutely sensitizes cells co-expressing HER2 and HR PIK3CA. (**A**) Percent cells (MCF10A/HER2/WT vs HR PIK3CA) survived following 25nM 17-AAG treatment with or without serum/growth factors in 2D growth assay. (**B**) Microscopic images (10×) of MCF10A/HER2/HR cells grown in 3D and as spheres in the absence and presence of 25 nM 17-AAG. (**C**) Immunoblot for HSP90 and HSP70 levels following 17-AAG treatment in MCF10A/HER2/HR cells. Tubulin was used as a loading control. (**D**) Microscopic images (10×) showing effects of HSP90 knock-down on 3D growth and mammosphere formation in MCF10A/HER2/HR cells. (**E**) Immunoblot detecting changes in HER2 and HER3 (total and phosphorylated) as well as IL-6 and HRG levels in siHSP90-transfected MCF10A/HER2/HR cells. (**F**) Average tumor volumes of nude mice transplanted with HCC1954 cells and treated with (four mice) or without (six mice) 17-AAG for 4 weeks. Mice were i.p. injected with 50 mg/kg 17-AAG from fourth to seventh days in week 1, followed by 25 mg/kg thrice a week for remaining 3 weeks. (**G**) Immunoblot with control and 17-AAG-treated tumor extracts measuring HSP70, HRG and IL-6 levels. (**H**) ELISA for detection of human IL-6 and IL8 levels in 17-AAG-treated or untreated mice sera. (**I**) Schematics explaining the evolution of HER2 and HR PIK3CA-co-expressing tumors from mammary epithelial cells. Bar graphs in (A) and (H) represent average values of triplicates plus standard errors.

Discussion

The aim of this study was to uncover the molecular interaction(s) between the *HER2* and *HR PIK3CA* oncogenes. Using isogenic cell line models representing *HER2*-amplified and WT or HR-mutated PIK3CA-expressing mammary epithelial cells, we found a causal association between the mutated oncogene and gain of phenotypic and functional properties of typical BCSCs in HER2+ cells (Figure 1A–F). This was further extended to BC cells (BT-20 and T47-D) carrying both molecular alterations (Supplementary

Figure S1, available at *Carcinogenesis* online) and attributed to the mutant protein (PIK3CA) (Supplementary Figure S2, available at *Carcinogenesis* online). We also provided evidences for EMT and cytokine (having functions as diverse as inflammation, angiogenesis, stem cell maintenance, migration and invasion) secretion by these cells (Figures 2 and 3). Some of these functional and phenotypic properties were also captured at the gene expression levels (Supplementary Tables S2 and S3, available at *Carcinogenesis* online).

While searching for an explanation for the *HR PIK3CA* oncogene bestowing several characteristics of aggressive BC in HER2+ mammary epithelial cells, we found signs of modest oxidative stress-associated DNA damage and phenotypes resembling oncogene-induced senescence (Figure 4E–N). Oxidative stress-associated oncogene-induced senescence typically triggers permanent growth arrest in oncogene-inflicted cells. However, HER2/HR cells continue to proliferate, which could partly be due to resetting of cellular redox balance (Figure 4O) and/or "stemness" promoting functions of HR secretome (Figure 5B–E).

In vivo, SASP helps immune clearance of senescent cells (40). The fact that the HER2/HR-specific secretome attracted more immune cells from peripheral blood than that from the matched WT control (Figure 5F) is a further validation for its resemblance with SASP. It also supports the previously reported association between *PIK3CA* oncogenic mutations and high number of tumor-infiltrating CD8+T and NK cells in clinical samples (48). Despite attracting more immune cells toward mutant cells, HR secretome prevented their clearance (Figure 5G and Supplementary Figure S8, available at *Carcinogenesis* online). This is similar to the function of SASP in immune evasion (40).

Production of SASP is a highly dynamic, context-dependent phenomenon affecting tumor recurrence, metastasis and drug efficacy (40,49). Based on the similarities between the HR secretome and SASP, it is thus possible that HER2+ tumors expressing this oncogene behave differently in different patients owing to inter-tumor heterogeneity and differences in tumor microenvironment. These are too complex to capture in simple pre-clinical models and may be responsible for anomalous behavior of these tumors between laboratory and clinical settings.

Finally, from a therapeutic perspective, we identified the HER2/HR-specific gene signature negatively correlated with that from cells treated with HSP90 inhibitor (Supplementary Table S4, available at *Carcinogenesis* online). Also, recent study demonstrated HSP90 inhibitors capable of eradicating senescent cells (50). Both of these were not only confirmed in the HER2/HR+ mammary epithelial and BC cells (Figure 6 and Supplementary Figure S10, available at *Carcinogenesis* online), but also indicated a specific way of inhibiting this subtype of BC. Notably, HSP90 inhibition has been proved to be quite promising for patients with trastuzumab-refractory, HER2+ metastatic BC, fraction of which could represent PIK3CA-mutated tumors (51).

Based on our findings, we have proposed an evolutionary model of breast tumorigenesis from mammary epithelial cells with amplified *HER2* and *HR*-mutated *PIK3CA* oncogenes (Figure 6I). Gain of mutated oncogene triggers HER2+ cell hyperproliferation resulting in excessive ROS production, persistent DNA-damage response and activation of NF-κβ signaling pathway. These endow these cells a senescence-like state characterized by secretion of various factors like conventional SASP. Initially, the secretome keeps tumorigenesis in check by enforcing and maintaining senescence-like state in neighboring cells and/or promoting immune-mediated clearance of oncogene-transformed cells. Simultaneously, these cells reset their redox balance to minimize the oxidative stress and regain proliferative capacity. Later, however, the detrimental effects of HR secretome (promotion of migration, invasion, stem-cell enrichment and evasion of immune surveillance) become predominant, resuming tumor progression. Thus, from a tumor cell's perspective, maintaining a secretome-producing senescence-like phenotype provides an evolutionary fitter strategy. This, in turn, renders these tumors vulnerable to inhibition of HSP90 chaperone function. Interaction among the tumor secretome and host microenvironment is radically different in patients and hence contribute to their clinical behaviors and trastuzumab sensitivity. Recapitulating such progressive evolution is not a simple task in any of the existing pre-clinical models since the *in vitro* models lack tumor microenvironment that in the *in vivo* models cannot be fully functional due to species differences between the secretome and their interacting partners in the rodent host.

Supplementary material

Supplementary data are available at *Carcinogenesis* online.

Funding

Department of Science and Technology (ECR/2015/000198 to A.C. and ECR/2015/000197 to G.C. and A.C.); Department of Biotechnology (BT/HRD/35/02/2006 to A.C. and BT/RLF/RE-ENTRY/18/2013 to G.C.); Shiv Nadar University.

Acknowledgements

The authors thank Ms. Teresa Dugger (Vanderbilt University Medical Center, USA) for technical help in animal studies and Dr. Kausik Chakraborty (CSIR-IGIB, New Delhi, India) for performing camp analysis.
Conflict of Interest Statement: None declared.

References

1. Slamon, D.J. *et al.* (1987) Human breast cancer: correlation of relapse and survival with amplification of the HER-2/neu oncogene. *Science*, 235, 177–182.
2. Moasser, M.M. (2007) The oncogene HER2: its signaling and transforming functions and its role in human cancer pathogenesis. *Oncogene*, 26, 6469–6487.
3. Fruman, D.A. *et al.* (2017) The PI3K pathway in human disease. *Cell*, 170, 605–635.
4. Cisowskia, J. *et al.* (2016) What makes oncogenes mutually exclusive? *Small GTPases*, 8, 187–192.
5. Network, T.C.G.A. (2012) Comprehensive molecular portraits of human breast tumours. *Nature*, 490, 61–70.
6. Samuels, Y. *et al.* (2004) High frequency of mutations of the PIK3CA gene in human cancers. *Science*, 304, 554.
7. Chakrabarty, A. *et al.* (2010) H1047R phosphatidylinositol 3-kinase mutant enhances HER2-mediated transformation by heregulin production and activation of HER3. *Oncogene*, 29, 5193–5203.
8. Hanker, A.B. *et al.* (2013) Mutant PIK3CA accelerates HER2-driven transgenic mammary tumors and induces resistance to combinations of anti-HER2 therapies. *Proc. Natl Acad. Sci. USA*, 110, 14372–14377.
9. Loibl, S. *et al.* (2016) PIK3CA mutations are associated with reduced pathological complete response rates in primary HER2-positive breast cancer: pooled analysis of 967 patients from five prospective trials investigating lapatinib and trastuzumab. *Ann. Oncol.*, 27, 1519–1525.
10. Wani, T.H. *et al.* (2018) Adaptation to chronic exposure to sepantronium bromide (YM155), a prototypical survivin suppressant is due to persistent DNA damage-response in breast cancer cells. *Oncotarget*, 9, 33589–33600.

11. Artym, V.V. *et al.* (2006) Dynamic interactions of cortactin and membrane type 1 matrix metalloproteinase at invadopodia: defining the stages of invadopodia formation and function. *Cancer Res.*, 66, 3034–3043.
12. Ricardo, S. *et al.* (2011) Breast cancer stem cell markers CD44, CD24 and ALDH1: expression distribution within intrinsic molecular subtype. *J. Clin. Pathol.*, 64, 937–946.
13. Pastrana, E. *et al.* (2011) Eyes wide open: a critical review of sphere-formation as an assay for stem cells. *Cell Stem Cell*, 8, 486–498.
14. Debnath, J. *et al.* (2003) Morphogenesis and oncogenesis of MCF-10A mammary epithelial acini grown in three-dimensional basement membrane cultures. *Methods*, 30, 256–268.
15. Hinohara, K. *et al.* (2012) ErbB receptor tyrosine kinase/NF-κB signaling controls mammosphere formation in human breast cancer. *Proc. Natl Acad. Sci. USA*, 109, 6584–6589.
16. Kim, J. *et al.* (2012) Tumor initiating but differentiated luminal-like breast cancer cells are highly invasive in the absence of basal-like activity. *Proc. Natl Acad. Sci. USA*, 109, 6124–6129.
17. Nakshatri, H. *et al.* (2009) Breast cancer stem cells and intrinsic subtypes: controversies rage on. *Curr. Stem Cell Res. Ther.*, 4, 50–60.
18. Ginestier, C. *et al.* (2007) ALDH1 is a marker of normal and malignant human mammary stem cells and a predictor of poor clinical outcome. *Cell Stem Cell*, 1, 555–567.
19. Magee, J.A. *et al.* (2012) Cancer stem cells: impact, heterogeneity, and uncertainty. *Cancer Cell*, 21, 283–296.
20. Mukherjee, B. *et al.* (2012) The dual PI3K/mTOR inhibitor NVP-BEZ235 is a potent inhibitor of ATM- and DNA-PKCs-mediated DNA damage responses. *Neoplasia*, 14, 34–43.
21. Sarker, D. *et al.* (2015) First-in-human phase I study of pictilisib (GDC-0941), a potent pan-class I phosphatidylinositol-3-kinase (PI3K) inhibitor, in patients with advanced solid tumors. *Clin. Cancer Res.*, 21, 77–86.
22. Thoreen, C.C. *et al.* (2009) An ATP-competitive mammalian target of rapamycin inhibitor reveals rapamycin-resistant functions of mTORC1. *J. Biol. Chem.*, 284, 8023–8032.
23. Maira, S.M. *et al.* (2008) Identification and characterization of NVP-BEZ235, a new orally available dual phosphatidylinositol 3-kinase/mammalian target of rapamycin inhibitor with potent *in vivo* antitumor activity. *Mol. Cancer Ther.*, 7, 1851–1863.
24. Mani, S.A. *et al.* (2008) The epithelial-mesenchymal transition generates cells with properties of stem cells. *Cell*, 133, 704–715.
25. Moreno-Bueno, G. *et al.* (2009) The morphological and molecular features of the epithelial-to-mesenchymal transition. *Nat. Protoc.*, 4, 1591–1613.
26. Tian, X. *et al.* (2011) E-cadherin/β-catenin complex and the epithelial barrier. *J. Biomed. Biotechnol.*, 2011, 567305.
27. Mongroo, P.S. *et al.* (2010) The role of the miR-200 family in epithelial-mesenchymal transition. *Cancer Biol. Ther.*, 10, 219–222.
28. Paz, H. *et al.* (2014) Invading one step at a time: the role of invadopodia in tumor metastasis. *Oncogene*, 33, 4193–4202.
29. Jacob, A. *et al.* (2015) The regulation of MMP targeting to invadopodia during cancer metastasis. *Front. Cell Dev. Biol.*, 3, 4.
30. Eckert, M.A. *et al.* (2011) Twist1-induced invadopodia formation promotes tumor metastasis. *Cancer Cell*, 19, 372–386.
31. Kessenbrock, K. *et al.* (2010) Matrix metalloproteinases: regulators of the tumor microenvironment. *Cell*, 141, 52–67.
32. Luo, M. *et al.* (2015) Epithelial-mesenchymal plasticity of breast cancer stem cells: implications for metastasis and therapeutic resistance. *Curr. Pharm. Des.*, 21, 1301–1310.
33. Hayes, D.F. *et al.*; Cancer and Leukemia Group B (CALGB) Investigators (2007) HER2 and response to paclitaxel in node-positive breast cancer. *N. Engl. J. Med.*, 357, 1496–1506.
34. Fonsecaa, N.A. *et al.* (2017) The cancer stem cell phenotype as a determinant factor of the heterotypic nature of breast tumors. *Crit. Rev. Oncol./Hematol.*, 113, 111–121.
35. Bellomo, C. *et al.* (2016) Transforming growth factor β as regulator of cancer stemness and metastasis. *Br. J. Cancer*, 115, 761–769.
36. Khalil, N. (1999) TGF-beta: from latent to active. *Microbes Infect.*, 1, 1255–1263.
37. Yingling, J.M. *et al.* (2018) Preclinical assessment of galunisertib (LY2157299 monohydrate), a first-in-class transforming growth factor-β receptor type I inhibitor. *Oncotarget*, 9, 6659–6677.
38. Chin, A.R. *et al.* (2014) Cytokines driving breast cancer stemness. *Mol. Cell. Endocrinol.*, 382, 598–602.
39. Kuilman, T. *et al.* (2010) The essence of senescence. *Genes Dev.*, 24, 2463–2479.
40. Coppé, J.P. *et al.* (2010) The senescence-associated secretory phenotype: the dark side of tumor suppression. *Annu. Rev. Pathol.*, 5, 99–118.
41. Zhao, H. *et al.* (2010) New biomarkers probing depth of cell senescence assessed by laser scanning cytometry. *Cytometry A*, 77, 999–1007.
42. Courtois-Cox, S. *et al.* (2008) Many roads lead to oncogene-induced senescence. *Oncogene*, 27, 2801–2809.
43. Kasai, H. (1997) Analysis of a form of oxidative DNA damage, 8-hydroxy-2'-deoxyguanosine, as a marker of cellular oxidative stress during carcinogenesis. *Mutat. Res.*, 387, 147–163.
44. Nelson, G. *et al.* (2012) A senescent cell bystander effect: senescence-induced senescence. *Aging Cell*, 11, 345–349.
45. Arteaga, C.L. *et al.* (2011) Treatment of HER2-positive breast cancer: current status and future perspectives. *Nat. Rev. Clin. Oncol.*, 9, 16–32.
46. Lamb, J. *et al.* (2006) The Connectivity Map: using gene-expression signatures to connect small molecules, genes, and disease. *Science*, 313, 1929–1935.
47. Workman, P. (2003) Auditing the pharmacological accounts for Hsp90 molecular chaperone inhibitors: unfolding the relationship between pharmacokinetics and pharmacodynamics. *Mol. Cancer Ther.*, 2, 131–138.
48. Siemers, N.O. *et al.* (2017) Genome-wide association analysis identifies genetic correlates of immune infiltrates in solid tumors. *PLoS One*, 12, e0179726.
49. Salama, R. *et al.* (2014) Cellular senescence and its effector programs. *Genes Dev.*, 28, 99–114.
50. Fuhrmann-Stroissnigg, H. *et al.* (2017) Identification of HSP90 inhibitors as a novel class of senolytics. *Nat. Commun.*, 8, 422.
51. Modi, S. *et al.* (2011) HSP90 inhibition is effective in breast cancer: a phase II trial of tanespimycin (17-AAG) plus trastuzumab in patients with HER2-positive metastatic breast cancer progressing on trastuzumab. *Clin. Cancer Res.*, 17, 5132–5139.